Invasive Species Mapping in Hawaiian Rainforests Using Multi-Temporal Hyperion Spaceborne Imaging Spectroscopy

Ben Somers and Gregory P. Asner

***Abstract*—We evaluated the potential of multi-temporal Multiple Endmember Spectral Mixture Analysis (MESMA) of Earth Observing-1 Hyperion data for detection of invasive tree species in the montane rainforest area of the Hawaii Volcanoes National Park, Island of Hawaii. We observed a clear seasonal trend in invasive species detection success when unmixing results were cross-referenced to ground observations; with Kappa coefficients (indicating detection success, 0–1) ranging between 0.66 (summer) and 0.69 (winter) and 0.51–0.53 during seasonal transition periods. An increase of Kappa to 0.80 was observed when spectral features extracted from September, August and January were integrated into MESMA. Multi-temporal unmixing improved the detection success of invasive species because spectral information acquired over different portions of the growing season allowed us to capture species-specific phenology, thereby reducing spectral similarity among species.**

***Index Terms*—Earth Observing-1, Hawaii, Hyperion, InStability Index, MESMA, *Morella Faya*, phenology, temporal unmixing.**

I. Introduction

BOOSTED by human activities and movements across the planet, biological invasions are now viewed as a significant component of global change [1]. Remote sensing of invasive species is a critical component of conservation and management efforts, but reliable methods for the detection of invaders over large areas have not been widely established. Recently, airborne hyperspectral sensors have demonstrated potential for invasive species mapping across different types of communities and ecosystems (review by [2]), yet their relatively high cost and consequent lack of year-round monitoring are known limitations for setting up a continuous monitoring program over large areas (review by [3]).

Manuscript received January 30, 2012; revised April 07, 2012 and April 26, 2012; accepted May 31, 2012. Date of publication July 17, 2012; date of current version May 13, 2013. The research presented in this paper was funded by the Belgian Science Policy Office in the framework of the STEREO II Programme—Project VEGEMIX (SR/67/146). The Carnegie Airborne Observatory is supported by the W. M. Keck Foundation, the Gordon and Betty Moore Foundation, the Grantham Foundation for the Protection of the Environment, and William Hearst III. This study was supported by a grant from the NASA Terrestrial Ecology Program, and by NSF grant DEB-0715593.

B. Somers is with the Flemish Institute for Technological Research (VITO), Centre for Remote Sensing and Earth Observation Processes (TAP), BE-2400 Mol, Belgium.

G. P. Asner is with the Department of Global Ecology, Carnegie Institution for Science, Stanford, CA 94305 USA.

Color versions of one or more of the figures in this paper are available online at http://ieeexplore.ieee.org.

Digital Object Identifier 10.1109/JSTARS.2012.2203796

The deployment of satellite-based hyperspectral sensors such as the Earth Observing-1 Hyperion might provide a powerful alternative. Although the frequent revisits and high spectral resolution are very promising, Hyperion's ground sampling distance of 30 m results in image pixels composed of mixtures of different ground components (e.g. invasive species, native species, soil, shadow), limiting the sensor's potential for invasive species detection [3], [30]. Many spectral unmixing approaches or sub-pixel classification techniques have been presented, but their accuracy remains moderate when dealing with mixtures composed of highly similar endmembers (reviewed by [4]). Because of this within-pixel spectral mixing, the utility of high spectral resolution satellite imagery for detecting and mapping invasive species seems limited [2]. Yet Hyperion has the capability to cover large areas multiple times throughout a growing season. This temporal repeatability allows us to capture the phenological differences among plant species, which in turn, can aid in determining the best time to discriminate between targeted species and co-occurring native vegetation [5]. Imagery acquired during key phenological events may reduce spectral similarity issues and consequently improve overall detection and mapping accuracy. While this hypothesis has been acknowledged by many, very few studies of spectral separability using seasonal data have been published. Dennison and Roberts [6] studied the effects of vegetation phenology on species mapping in chaparral, while recently Hesketh and Sanchez-Azofeifa [7] evaluated how season impacts leaf level spectral separability in Costa Rican seasonally dry forests.

Here we explore the potential of Multiple Endmember Spectral Mixture Analysis (MESMA, [8])—a commonly used sub-pixel classification technique—for detecting patches of the invasive nitrogen (N)-fixing *Morella faya* tree in the montane rainforests of Hawaii Volcanoes National Park, Island of Hawaii. A Hyperion time series composed of 18 cloud-free images spanning a period of four years was prepared. The main objective was to evaluate whether the invasive species can be detected more effectively when spectral information acquired over different spectral regions (visible, VIS; near-infrared, NIR; and shortwave infrared, SWIR) and different segments of the growing season are assimilated into MESMA. This is a novel approach—to build a single, composite image representing the entire year, drawing upon the spectral wavelength ranges most useful per season for species differentiation, from a time series developed from images collected over several years. The hypothesis is that spectral similarity problems between species can be overcome by taking advantage of seasonal variation in

their spectroscopic reflectance signatures, resulting in more effective detection of the invaders. Finally, we investigated whether a seasonal trend in the accuracy of invasive species detection could be developed for *Morella faya* in Hawaii. This aspect of the study is key to identifying the best time to monitor changes in invasive species extent over time, which would enable us to target aircraft assets more cost effectively.

II. Materials and Methods

A. Study Area

Although being a global threat, the destructive effects of invasive species are perhaps most pronounced in island ecosystems [9], [10]. This study was therefore conducted in the Hawaii Volcanoes National Park on the Island of Hawaii (Fig. 1, top panel). The study focused on a 300 ha rainforest ecosystem ($19^\circ\ 24'\ 00''\ \mathrm{N}, 115^\circ\ 14'\ 50''\ \mathrm{W}$) characterized by a patchy mosaic of two dominant overstory species—the highly invasive N-fixing *Morella faya* (Ait.) and common native Hawaiian *Metrosideros polymorpha* (Gaud.) (Fig. 1, bottom panel). Ground-based measurements show that *Metrosideros* forests in this area have an understory dominated by tree ferns (especially *Cibotium glaucum*); the trees are approximately 15–20 m tall with high leaf area index (LAI, 3–6) but low leaf N (0.7–0.85%) and low water content (45–55%, mass basis). In contrast, the invasive *Morella* stands contain almost no understory plants due to dense shading from very high LAI (5–10) [11], and trees have high leaf N (1.5–1.9%) and moderate water content (50–65%) [12]. *Morella faya* causes enormous changes in the nutrient balance and structure of the native *Metrosideros* forests, and is therefore seen as one of the main threats to the native fauna and flora [13].

B. Hyperion Time Series

The EO-1 Hyperion instrument collects spectra in 220 wavebands ranging from 400 to 2500 nm at a spatial resolution of 30 m. Beginning in July 2004 and running through December 2007 (with an interruption for the second half of 2006), Hyperion was tasked for data collections on approximately a weekly basis over the study area. The resulting data set was subsequently limited to 18 cloud-free scenes covering the study area (Table I). Most cloud-free images acquired over the study area were obtained in winter (January–February) or summer (July–October) months, corresponding to the two drier times of year [14]. The time series data were geo-referenced and radiometrically preprocessed at the Carnegie Institution for Science, Stanford, California. Each Hyperion image was processed to apparent surface reflectance using the ACORN-5LiBatch (Imspec LLC, Palmdale, CA) atmospheric correction model. The visibility was set to 50 km and water vapor was retrieved using the 940 and 1060 nm water absorption bands as per the ACORN method. No ground calibration was used. A destriping algorithm was then applied to compensate for miscalibration between cross-track detectors. A cubic spline curve was fitted to the water bands at 940 and 1140 nm in each pixel to reduce effects of miscalibration and modeling errors introduced by atmospheric correction. Full details on the preprocessing chain can be found in [15]. Due to the low signal to noise ratio (SNR), the spectral information in the wavelengths between 1800–2500 nm was not considered in further analysis.

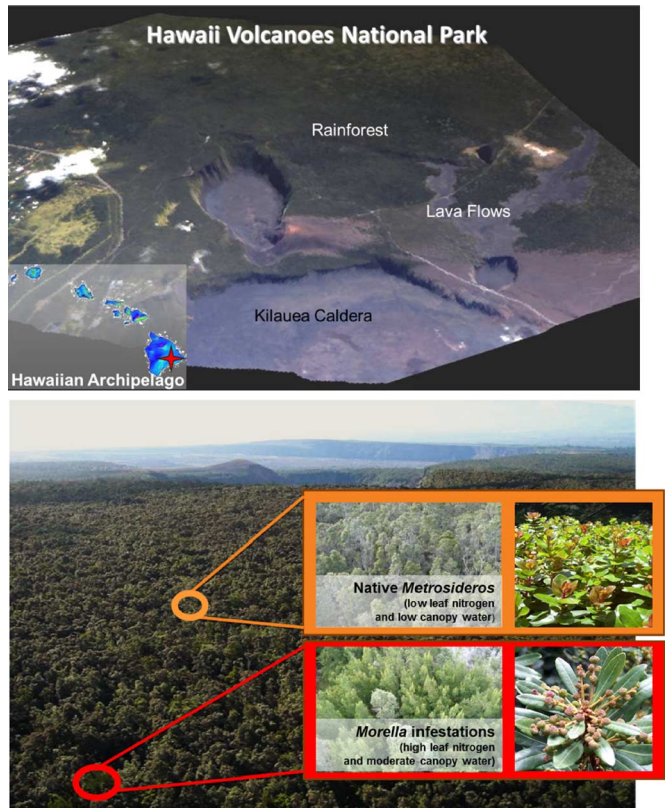

Fig. 1. (Top) Overview of the Hawaii Volcanoes National Park on the Island of Hawaii (imagery from the Carnegie Airborne Observatory; [29]); (Bottom) Detail of the native ohia (*Metrosideros*) forests. Although most of this area is under protection by the U.S. National Park Service, it has experienced a number of biological invasions, predominantly by *Morella faya*.

TABLE I
EO-1 Hyperion Imagery Compiled Into Time Series for This Study

	2004	2005	2006	2007	
January		XX	X	X	3/3
February			X		1/3
March		X			1/3
April					0/3
May					0/3
June			X		1/3
July		X		X	2/3
August	XX	XX			2/3
September	XX				1/3
October	XX			X	2/3
November					0/3
December					0/3
total/yr	6	6	3	3	

C. Ground Control Points

A set of 60 field observations of tree species locations (27 for *Morella faya* and 33 for *Metrosideros polymorpha*; average uncertainty of ~2 m) is available for this study. These field data

were acquired in January 2005 and were used as the validation set for evaluating the invasive species detection success of MESMA.

D. Morella Versus Metrosideros

Exploring the potential of Hyperion time series to aid the detection and mapping of *Morella* infestations first requires identification of the best times in the growing season to differentiate both species. Characteristic spectral endmember libraries were collected for both *Morella* and *Metrosideros*. Through a combination of field observations and an airborne, very high-resolution image dataset [12], patches with approximately 100% *Morella* cover or *Metrosideros* were identified. Pixels within these patches were selected to extract species-specific spectral information from the Hyperion time series. These time series then allowed for an evaluation of the typical phenological changes between the two species throughout the growing season, as was already presented by [5] for a shorter Hyperion time series.

For each time step, the spectral separability between both species' libraries was quantified using the InStability Index (ISI, [16], [17]), defined as the ratio of the within-class variability and the between-class variability:

$$ISI_i = \frac{\Delta_{within,i}}{\Delta_{between,i}} = \frac{1.96 \times (\sigma_{1,i} + \sigma_{2,i})}{|R_{mean,1,i} - R_{mean,2,i}|} \quad (1)$$

where $R_{mean,1,i}$ and $R_{mean,2,i}$ are the mean reflectance values at wavelength i for endmember class 1 and endmember class 2, respectively, whereas $\sigma_{1,i}$ and $\sigma_{2,i}$ are the standard deviations of class 1 and 2, respectively. Lower ISI values indicate better separability of the species in the specified waveband.

E. Invasive Species Detection

The validation set of tree locations described in Section II-C was acquired in January 2005. We therefore only used the images from August 2004 through July 2005 to cross-reference classification results to the ground observations. This resulted in a time series of six images acquired in August/September/October 2004 and January/March/July 2005 that were used in further analysis.

Each Hyperion reflectance image was translated into sub-pixel cover fraction maps of *Metrosideros* and *Morella* using the MESMA approach [8]. MESMA models a mixed spectrum as a combination of its constituent spectral components or endmembers (e.g., native and invasive tree species) weighted by their fractional cover in the pixel:

$$r = \mathbf{M}f + \varepsilon \quad \text{with} \quad \sum_{j=0}^{m} f_j \quad \text{and} \quad 0 \le f_j \le 1 \quad (2)$$

where $\mathbf{M}$ is a $n \times m$ matrix of which each column corresponds to the spectral signal of a specific endmember or ground cover class and each row corresponds to a specific waveband. f is a column vector $[f_1, \ldots, f_m]^{\mathrm{T}}$ that denotes the sub-pixel cover fractions occupied by each of the m endmembers in the pixel. The portion of the spectrum that cannot be modeled is expressed as a residual term, ε. Sub-pixel endmember fractions are obtained by solving for the corresponding vector f such that the following equation is minimized within the constraints of (2):

$$f = \sum_{i=1}^{n} \varepsilon_i^2 = \|\mathbf{M}f - r\|^2 \quad (3)$$

Unlike most of the traditional unmixing approaches, MESMA allows the endmember matrix $\mathbf{M}$ to vary on a per pixel basis. This enables modeling of the inherent spectral variability within an image scene [4], [8]. For each run, different endmember combinations, randomly selected from a spectral library, are used to decompose each pixel. The model with the best fit, i.e. with the lowest root mean square error (RMSE) in the reconstruction of the original pixel, is adopted. The species-specific spectral libraries for *Morella faya* and *Metrosideros polymorpha* described in Section II-D were used as input for our MESMA runs. Note that we did not use a separate shade endmember in the unmixing process, but rather treated it as an integral part of the spectral properties of each species [18].

F. Multi-Temporal Unmixing

The Hyperion time series provided a means to capture the phenological differences among the native and invasive tree species. Therefore, by assimilating spectral information from different spectral regions that were acquired over different periods of the growing season, the spectral separability between both endmember classes could be maximized. Such a multi-temporal and synthetic spectral construction using the MESMA approach should result in a more effective detection of invasive species.

First, the ISI spectrum was calculated for each image of the time series. Second, for each typical spectral region, the image that provided the best separability between *Metrosideros* and *Morella*, as indicated by the lowest ISI per spectral region among all images, was selected. The spectral regions were the VIS (400–700 nm), the NIR1 (710–1030 nm), the NIR2 (1043–1250 nm), and SWIR1 (1450–1800 nm; SWIR2 was discarded, 1800–2500 nm).

As such, an image cube was built that was composed of spectral information originating from different individual images. In other words, a new image was created for which the spectral profiles were now composed of reflectance values of different periods of the growing season but for which the spectral separability between the endmembers was maximized. This image captured the seasonal phenology per spectral region in the most responsive months, and represents a new way to integrate time-series spectral imagery for ecological study. Finally, the composited image was used as input into MESMA.

III. Results and Discussion

A. Morella Versus Metrosideros

A monthly comparison of endmember libraries for *Metrosideros* and *Morella* is shown in Fig. 2, compiled from the 18 cloud-free images (see Section II-D.) which show the monthly means and 95% confidence intervals of the spectral libraries. A clear seasonal effect, with reflectance values progressively increasing towards the summer months, could be observed.

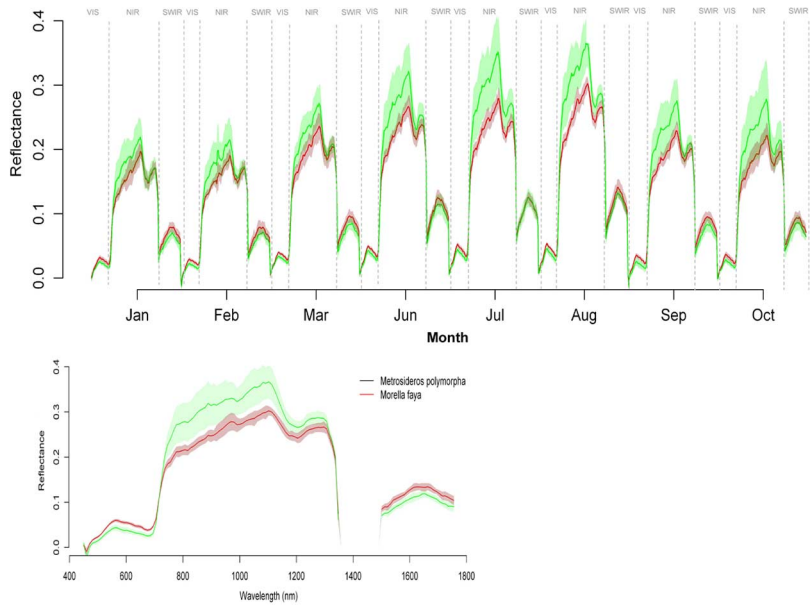

Fig. 2. Top panel: Temporal evolution of the mean and 95% confidence interval of the native *Metrosideros* (darker line and shading) and invader *Morella* (lighter line and shading) endmember libraries (see Section II-D.). Spectra are shown for eight months, each of which display the VIS, NIR, and SWIR1 wavelengths (400–1800 nm). Bottom panel: Composite spectral profile showing maximum separability between both endmember classes. The composite spectrum is composed of spectral information from September (VIS), August (NIR1, NIR2) and January (SWIR1), all of which had the lowest InStability Index (ISI) per spectral region and month.

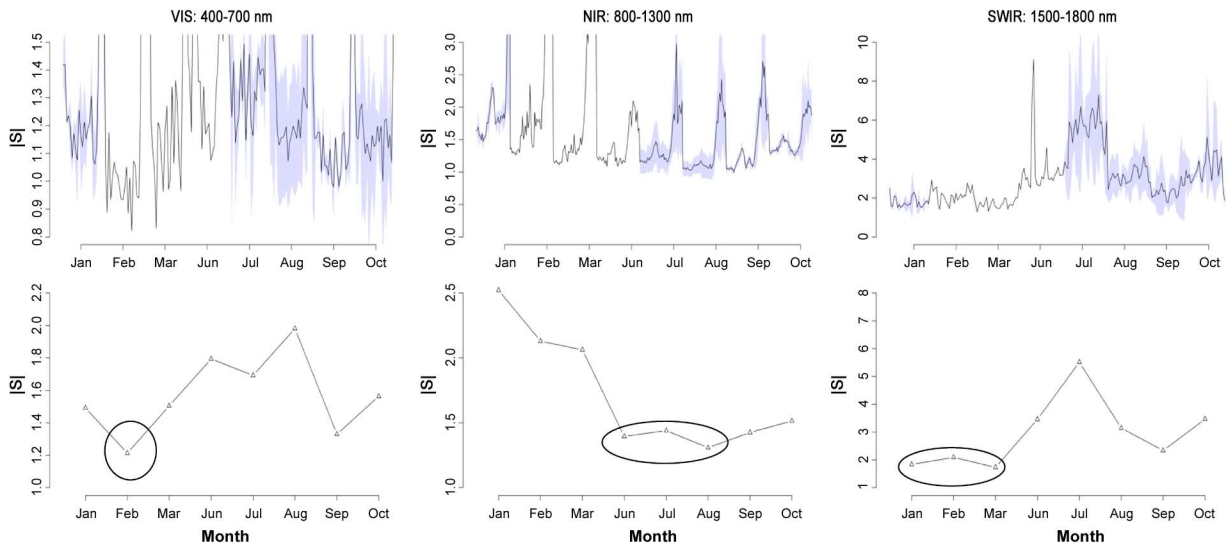

Fig. 3. Temporal evolution of ISI for VIS, NIR and SWIR1. Results are compiled from the time series of species specific endmember libraries as extracted from the 18 cloud-free images (see Section II-D.). While the top panels show the wavelength specific monthly means and 95% confidence interval, the bottom panels show the overall monthly means for the entire VIS (left), NIR (middle) and SWIR1 (right) domains. The months having the lowest InStability Index (ISI) (i.e., best discrimination) are circled.

The higher NIR reflectance for the invasive species is apparent, whereas the VIS and SWIR1 reflectance is higher for the native species, throughout the year. This effect was previously observed with a shorter Hyperion time series [5]. In this study, however, we are mainly interested in the evolution of the spectral separability between both species over time, as determined using ISI (Fig. 3).

In the VIS, we observed that both species are most similar with high ISI in summer months while they are most dissimilar (with low ISI) during seasonal transitions, e.g., February and September. In the NIR, the separability between species progressively increases towards the summer period while declining again in autumn and winter. This confirms the earlier results [5] which showed a similar trend in LAI over a shorter time series. For the SWIR1, we observed the opposite trend, with poor separability in summer and greater separability in winter. This can be explained by the fact that in the summer months, *Morella faya* produces more photosynthetically active leaves. Meanwhile, *Metrosideros* is a slow-growing hardwood native with a relatively stable canopy all year long, with only some minor increases in LAI in the summer ($\sim$1/2 LAI unit) [5]. This can also be observed in Fig. 2 where the intra-class variability of

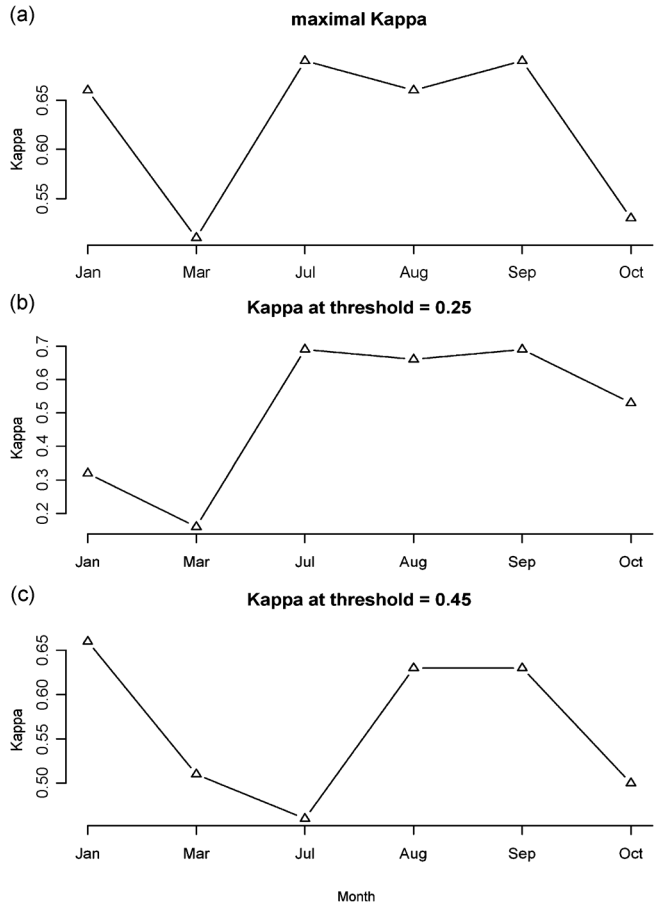

Fig. 4. The seasonal trend in the success of detecting *Morella* invasions. The sub-pixel maps of *Morella* cover as provided by MESMA were cross-referenced to the field observations of known tree positions (see Section II-C) through a hard classification approach. In the hard classification all sub-pixel cover fraction values exceeding a predefined threshold were assigned to *Morella*, all fraction values below this threshold were assigned to *Metrosideros*. Results show the detection success expressed as the Cohen's Kappa coefficient. Top panel: The highest Kappa per month obtained in all available images is shown. Middle Panel: The optimal classification accuracy for July/August/September/October images using a MESMA threshold of 25% is shown. Bottom Panel: The optimal classification accuracy for January/March images using a MESMA threshold of 45% is shown.

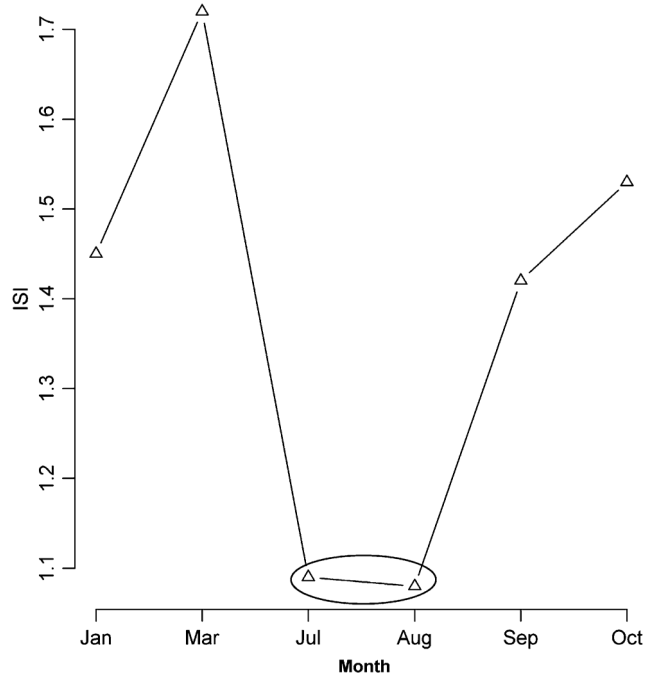

Fig. 5. Seasonal trend in the average InStability Index (ISI). The best discrimination between species was obtained in July and August (circled).

Metrosideros is much lower than that of *Morella*. The enhanced separability in the winter for both the SWIR1, and to a lesser extent the VIS (Fig. 2), is related to yellowing of *Morella* leaves due to unfavorable low sun conditions (Fig. 2) at a time when precipitation is high (G. Asner, *unpub. data*).

This analysis reveals a clear seasonal trend in the separability of *Morella* and *Metrosideros*. It should, however, be noted that not all months were equally represented in the analysis and that inter-seasonal changes might result in small shifts in phenology, and consequently in spectral separability among years.

B. Invasive Species Detection

The seasonal trend in the success of detecting *Morella* invasions was studied based on a time series of six images acquired in August/September/October 2004 and January/March/July 2005. The sub-pixel cover maps of *Morella* provided by MESMA were cross-referenced to the field observations of known tree positions (see Section II-C) through a "hard" classification approach [18], i.e. all sub-pixel cover fraction values exceeding a predefined threshold were assigned to *Morella*, all fraction values below this threshold were assigned to *Metrosideros*. Results are summarized in Figs. 4 and 6, showing a distinct seasonal trend in detection success, with highest Kappa coefficients in summer and winter months and clearly lower values in March and October. The best accuracies ($\mathrm{Kappa} = 0.69$) were observed in July and September (Figs. 4 and 6). The decrease in accuracy for March and October can be attributed to increased spectral similarity between the two species as demonstrated in Fig. 5, as an increase in average ISI. Fig. 6 shows that optimal Kappa values for the summer period (July–October) were obtained for a MESMA threshold around 25% (i.e., in the hard classification, all cover fraction values exceeding this threshold were assigned to *Morella*, all fraction values below this threshold were assigned to *Metrosideros*), while a shift towards 45% was observed for March and January.

Although these results were compiled to obtain a single, average growing season spectrum, the analysis indicates that the seasonal transition periods (from summer to winter and vice versa) are not favorable for detection of *Morella faya*. In Hawaii, these correspond to periods when cloud-free images are rarely available from EO-1 (see Table I) or from other optical sensors such as Landsat [19].

C. Multi-Temporal Unmixing

Subsequently, we evaluated whether a multi-temporal unmixing approach can increase the detection success of *Morella*. Instead of evaluating ISI over time per spectral region, as in Fig. 3, we next evaluated ISI trends as a function of wavelength in each month (Fig. 7), with separate analysis per spectral region (VIS, NIR1, NIR2, SWIR1). Based on these ISI spectra, we selected the image providing the best separability between

TABLE II

KAPPA COEFFICIENTS FOR THE SINGLE DATE (KAPPA) AND MULTI-TEMPORAL MESMA CLASSIFICATIONS ($\mathrm{Kappa}_{\mathrm{temp}}$). FOR $\mathrm{Kappa}_{\mathrm{temp}}$ RESULTS ARE SHOWN FOR THE OPTIMAL OR MAXIMAL KAPPA ($\mathrm{Kappa}_{\mathrm{temp,MAX}}$), AND FOR THE MESMA HARD CLASSIFICATION THRESHOLDS 25% ($\mathrm{Kappa}_{\mathrm{temp,25\%}}$), 30% ($\mathrm{Kappa}_{\mathrm{temp,30\%}}$) AND 45% ($\mathrm{Kappa}_{\mathrm{temp,45\%}}$). $\mathrm{Threhold}_{\mathrm{MAX}}$ INDICATES THE THRESHOLD FOR WHICH $\mathrm{Kappa}_{\mathrm{temp,MAX}}$ IS ACHIEVED. IN THE $\mathrm{Kappa}_{\mathrm{temp}}$ COLUMNS, THE OPTIMAL KAPPA COEFFICIENT THAT COULD BE OBTAINED BY THE SINGLE DATE MESMA IS GIVEN AS A SUBSCRIPT IN PARENTHESES. THIS ALLOWS A FAST COMPARISON BETWEEN BOTH MESMA APPROACHES. FOR EACH SCENARIO, THE AVAILABLE IMAGES ARE INDICATED WITH AN 'x' AND FOR EACH SPECTRAL REGION (VIS, NIR1, NIR2, SWIR1) THE IMAGES THAT DEMONSTRATED THE BEST SEPARABILITY (LOWEST INSTABILITY INDEX, FIG. 7) BETWEEN *Morella* AND *Metrosideros* ARE SPECIFIED

	Jan	Mar	Jul	Aug	Sep	Oct	VIS	NIR1	NIR2	SWIR1	$\mathrm{Kappa}_{\mathrm{temp,MAX}}$	$\mathrm{Threshold}_{\mathrm{MAX}}$	$\mathrm{Kappa}_{\mathrm{temp,25\%}}$	$\mathrm{Kappa}_{\mathrm{temp,30\%}}$	$\mathrm{Kappa}_{\mathrm{temp,45\%}}$
6 images															
Kappa	0.66	0.51	0.69	0.66	0.69	0.53	Sep	Aug	Aug	Jan	$0.80_{(0.69)}$	41%-46%	$0.71_{(0.69)}$	$0.72_{(0.69)}$	$0.80_{(0.66)}$
4 images															
1	-	x	x	-	x	x	Sep	Jul	Jul	Sep	$0.70_{(0.69)}$	30%	$0.62_{(0.69)}$	$0.70_{(0.69)}$	$0.58_{(0.60)}$
2	x	x	-	-	x	x	Sep	Sep	Oct	Jan	$0.76_{(0.69)}$	29%	$0.73_{(0.69)}$	$0.76_{(0.56)}$	$0.39_{(0.66)}$
3	x	-	x	x	-	x	Oct	Aug	Aug	Jan	$0.76_{(0.69)}$	29%	$0.70_{(0.69)}$	$0.76_{(0.69)}$	$0.65_{(0.66)}$
4	-	x	x	x	-	x	Oct	Aug	Aug	Mar	$0.73_{(0.69)}$	25%	$0.73_{(0.69)}$	$0.63_{(0.69)}$	$0.61_{(0.61)}$
3 images															
5	-	x	-	-	x	x	Sep	Sep	Oct	Sep	$0.70_{(0.69)}$	32%	$0.62_{(0.69)}$	$0.70_{(0.56)}$	$0.51_{(0.60)}$
6	x	x	-	x	-	-	Mar	Aug	Aug	Jan	$0.73_{(0.66)}$	35%	$0.70_{(0.66)}$	$0.68_{(0.62)}$	$0.61_{(0.66)}$
7	x	-	x	x	-	-	Jan	Aug	Aug	Jan	$0.79_{(0.69)}$	33%	$0.69_{(0.69)}$	$0.76_{(0.69)}$	$0.76_{(0.66)}$
8	-	-	x	x	x	-	Sep	Aug	Aug	Sep	$0.75_{(0.69)}$	30%	$0.69_{(0.69)}$	$0.75_{(0.69)}$	$0.49_{(0.61)}$
2 images															
9	-	x	-	-	-	x	Oct	Mar	Oct	Mar	$0.60_{(0.53)}$	36%	$0.36_{(0.53)}$	$0.40_{(0.49)}$	$0.45_{(0.51)}$
10	-	-	x	x	-	-	Jul	Aug	Aug	Aug	$0.70_{(0.69)}$	30%	$0.66_{(0.69)}$	$0.70_{(0.69)}$	$0.61_{(0.61)}$

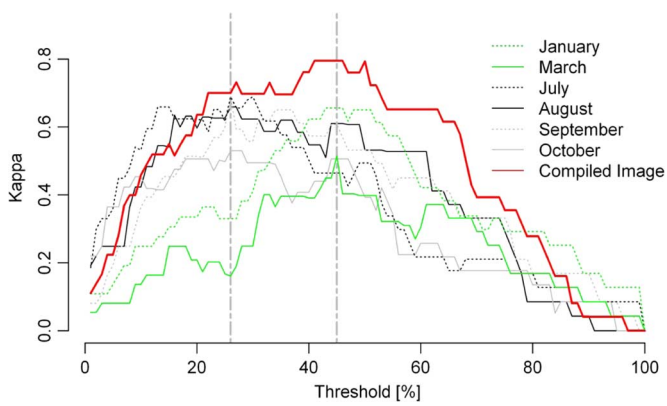

Fig. 6. The seasonal trends in the success of detecting *Morella* invasion, expressed as the Cohen's Kappa coefficient, as a function of the MESMA classification threshold, are shown for each month, as well as for the composite image from September (VIS), August (NIR1, NIR2) and January (SWIR1). The vertical dotted lines indicate the maximum Kappa values for thresholds of 45% (obtained in January/March) and 25% (obtained in July/August/September/October).

Metrosideros and *Morella* per spectral region, i.e., that image with the lowest average ISI per spectral region from the dataset. As such, an image cube as well as spectral endmember libraries of the spectral information from September (VIS), August (NIR1, NIR2) and January (SWIR1) were built and implemented in MESMA. The final, annual composite spectra for *Metrosideros* and *Morella* are shown in the bottom panel of Fig. 2.

Overall, the success of detecting *Morella* invasions was higher for the multi-temporal unmixing analysis compared to the single date approach. The optimal accuracies (the % pixels classified correctly, $\%\mathrm{correct} = 90$; %false positive observations, $\%\mathrm{FP} = 4$; %false negative observations, $\%\mathrm{FN} = 19$; $\mathrm{Kappa} = 0.80$) achieved at thresholds ranging between 41% to 46%, were clearly higher than the maximum accuracy that were achieved by the single date approach (e.g., for July and September, $\%\mathrm{correct} = 81$; $\%\mathrm{FP} = 19$; $\%\mathrm{FN} = 19$; $\mathrm{Kappa} = 0.69$; Fig. 6). Also at a threshold of 25%, representing the optimal Kappa observed for single date approaches in July/August/September/October (Fig. 6), the multi-temporal MESMA achieved a slightly higher Kappa (=0.71) compared to the single date approaches (Fig. 6).

In an operational setting, the set of available images can change from year to year, because of variable weather conditions (Table I). Therefore we tested the multi-temporal MESMA approach for 10 different (randomly selected) scenarios, drawing upon a different set of available images. This yielded a systematic increase of Kappa compared to the single date approaches (Table II) where the maximal Kappa for multi-temporal MESMA was higher than that achieved by a single date approach. This observation confirms the potential of multi-temporal unmixing for invasive species detection. Yet, the threshold associated with the maximal Kappa is strongly

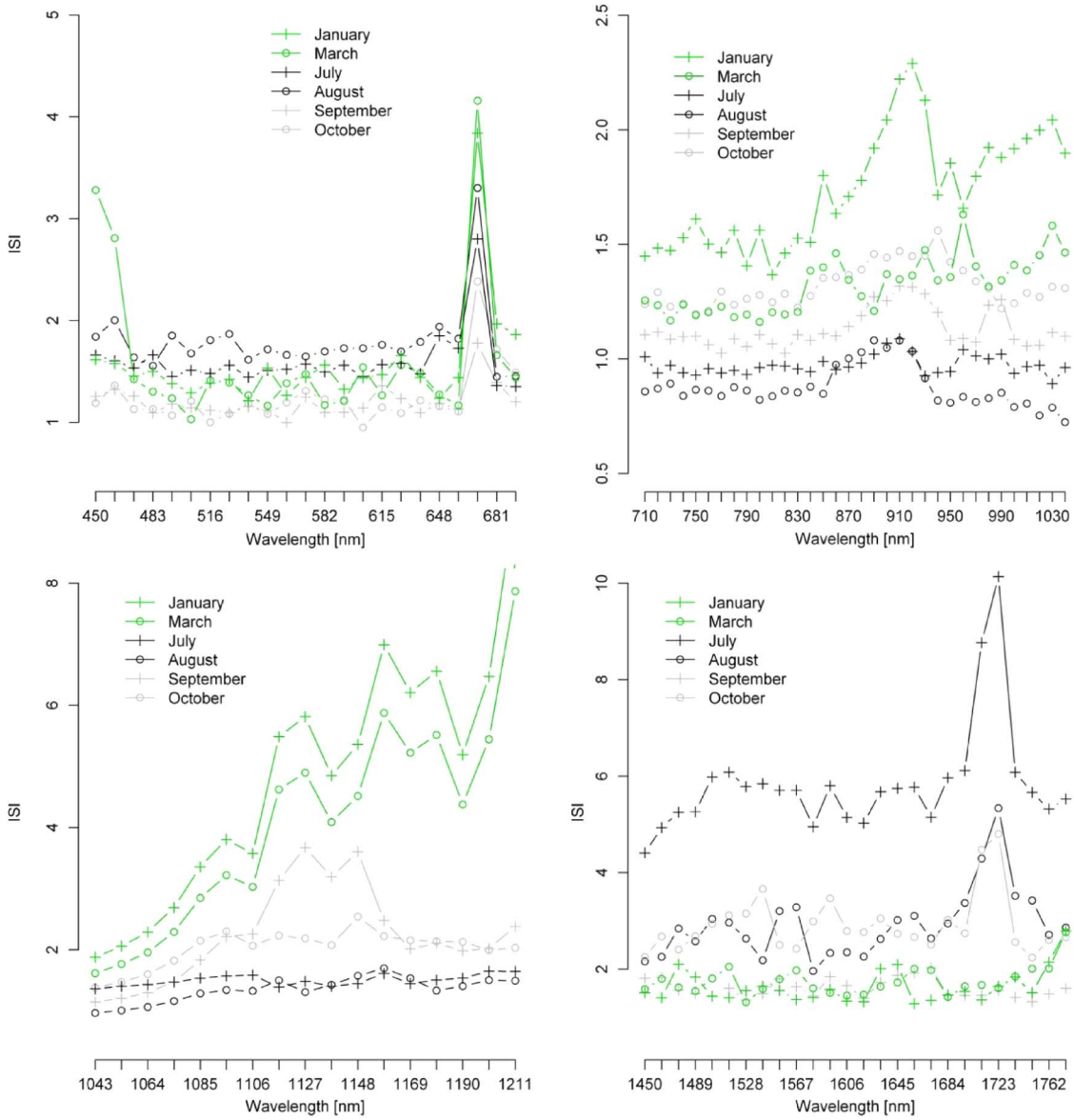

Fig. 7. InStability Index (ISI) spectra for the VIS, NIR1, NIR2, and SWIR1.

dependent upon the specific scenario. Generally, the optimum threshold ranges between 25% and 45%, similar to the optimal thresholds of the single date approaches (Fig. 6). For a threshold of 25% such as for the single data approaches of July-October (Fig. 6), the multiple unmixing approach for 6 of the 10 scenarios produced a Kappa equal to or higher than the single date approaches (Table II). For a threshold of 45% this success ratio dropped to 30% (with only one scenario showing an increase in Kappa for the multi-temporal approach; Table II). Overall, the best results were obtained for a threshold of 30% (Table II), for which the multi-temporal MESMA provided an improvement over the single date classifications in 80% of the cases.

IV. Conclusions

Here we tested the potential of the EO-1 Hyperion data for detection of patches of the invasive N-fixing *Morella faya* tree species in a montane rainforest area of the Hawaii Volcanoes National Park, Island of Hawaii. We developed a novel multi-step method that resulted in a composite image built from the four spectral regions (VIS, NIR1, NIR2, SWIR1), each taken from different months. First, implementation of MESMA on a time series of Hyperion images revealed a seasonal trend in the invasive species detection success. Summer and winter were the best time to discriminate between the invasive species versus the co-occurring native vegetation, while a clear decrease in classification accuracy was observed during the seasonal transition periods (from summer to winter and vice versa).

These seasonal dynamics provided opportunities for multi-temporal classification, which were successfully implemented using a multi-temporal MESMA approach. At this point, the separability of the two species in each month was assessed using the ISI for each spectral region. Then, the ISI values were used to discern the most favorable month per spectral range for differentiating the species, where low

ISI values indicated successful separation. The most useful combination of months and spectral regions for achieving this species separation were: VIS (September), NIR1 and NIR2 (August) and SWIR1 (January). These spectral/month sets were extracted from the full dataset and combined into a single composite image whereby a full spectrum was constructed from multi-seasonal data sources. This composite image was used to replace the time series and was ingested by MESMA.

This approach assimilates in MESMA spectral information from the different spectral regions acquired during different periods of the growing season. As such, species specific phenology was captured and spectral similarity problems were overcome, resulting in more effective detection of invasive species. It should be acknowledged that MESMA is driven by the availability of spectral endmember libraries. In our approach these libraries are used in an analysis of the temporal spectral separability of endmembers, which in turn, is used to build temporal spectral composites for implementation in MESMA. The approach is thus strongly dependent upon the availability and quality of the spectral endmember libraries. Ideally, the libraries should cover the spectral variability present in the image, which is not always feasible in highly heterogeneous scenes with strong environmental gradients or in cases where the number of available endmember spectra is limited. A potential solution is to automatically extract the endmembers from the image data using techniques such as those presented in [20], [21]. Current research is exploring the potential of these approaches for application in tropical rainforests [22].

We anticipate that the multi-temporal unmixing approach presented here will improve our ability to monitor the dynamics of target species in a heterogeneous or mixed canopy. Management practices in agricultural fields, forest and other natural ecosystems can benefit from this approach. Specific examples are: delineation of weed patches or crop canopies in agricultural fields for the site-specific application of farm inputs [23], the monitoring of understory vegetation dynamics and forest species distributions for forest health assessment [24], biodiversity management and conservation [25], mapping and characterization of grassland patches in mixed grassland ecosystems (savannas, woodlands, etc.) used to implement fire risk and fire severity control measures and grazing capacity/carrying capacity management [26]. Even in other research areas, like mineralogical studies or urban environments, the conceptual approaches to simultaneously reduce spectral similarity and mixing problems will have benefits [27], [28]. This hypothesis should, however, be tested through additional research. Ongoing research will evaluate the robustness of the approach for invasive species detection in other Hawaiian ecosystems including more complex sites dominated by more than two species.

ACKNOWLEDGMENT

The scientific input of Reinout Van Bets, Kristof Van Tricht, Roberta Martin, Laurent Tits, and David Knapp is gratefully acknowledged. We also thank the reviewers for their outstanding comments and suggestions, which greatly helped us to improve the technical content and presentation of our manuscript.

REFERENCES

[1] P. M. Vitousek, H. A. Mooney, J. Lubchenco, and J. M. Melillo, "Human domination of Earth's ecosystems," *Science*, vol. 277, pp. 494–499, 1997.

[2] K. S. He, D. Rocchini, M. Neteler, and H. Nagendra, "Benefits of hyperspectral remote sensing for tracking plant invasions," *Diversity and Distributions*, vol. 17, pp. 381–392, 2011.

[3] C. Huang and G. P. Asner, "Applications of remote sensing to alien invasive plant studies," *Sensors*, vol. 9, pp. 4869–4889, 2009.

[4] B. Somers, G. P. Asner, L. Tits, and P. Coppin, "Endmember variability in spectral mixture analysis: A review," *Remote Sens. Environ.*, vol. 115, pp. 1603–1616, 2011.

[5] G. P. Asner, R. E. Martin, K. M. Carlson, U. Rascher, and P. M. Vitousek, "Vegetation-climate interactions among native and invasive species in Hawaiian rainforest," *Ecosystems*, vol. 9, pp. 1041–1054, 2006.

[6] P. E. Dennison, P. E. , and D. A. Roberts, "The effects of vegetation phenology on endmember selection and species mapping in Southern California Chaparral," *Remote Sens. Environ.*, vol. 87, pp. 123–135, 2003.

[7] M. Hesketh and G. A. Sanchez-Azofeifa, "The effect of seasonal spectral variation on species classification in the Panamanian Tropical Forest," *Remote Sens. Environ.*, vol. 118, pp. 73–82.

[8] D. Roberts, M. Gardner, R. Church, S. Ustin, G. Scheer, and R. Green, "Mapping chaparral in the santa monica mountains using multiple endmember spectral mixture models," *Remote Sens. Environ.*, vol. 65, pp. 267–279, 1998.

[9] C. S. Elton, *The Ecology of Invasions by Animals and Plants*. London, U.K.: Methuen and Co., 1958.

[10] P. M. Vitousek, L. R. Walker, L. D. Whiteacre, D. Mueller-Dombois, and P. A. Matson, "Biological invasion by *Myrica faya* alters ecosystem development in Hawaii," *Science*, vol. 238, pp. 802–804, 1987.

[11] G. P. Asner, R. F. Hughes, P. M. Vitousek, D. E. Knapp, T. Kennedy-Bowdoin, J. Boardman, R. E. Martin, M. Eastwood, and R. O. Green, "Invasive plants transform the 3-D structure of rainforests," in *Proc. National Academy of Sciences of the United States of America*, 2008, vol. 105, pp. 4519–4523.

[12] G. P. Asner and P. M. Vitousek, "Remote analysis of biological invasion and biogeochemical change," in *Proc. National Academy of Sciences of the United States of America*, 2005, vol. 102, pp. 4383–4386.

[13] P. M. Vitousek and L. R. Walker, "Biological invasion by *Myrica faya* in Hawai'i: Plant demography, nitrogen fixation, ecosystem effects," *Ecological Monographs*, vol. 59, pp. 247–265, 1989.

[14] T. M. Giambelluca, M. A. Nullet, and T. A. Schroeder, "Rainfall Atlas of Hawaii," Dept. Land and Natural Resources, Honolulu, Hawaii, 1986.

[15] G. P. Asner and K. B. Heidebrecht, "Imaging spectroscopy for desertification studies: Comparing AVIRIS and EO-1 Hyperion in Argentina drylands," *IEEE Trans. Geosci. Remote Sens.*, vol. 41, pp. 1283–1296, 2003.

[16] B. Somers, S. Delalieux, W. Verstraeten, J. Van Aardt, G. Albrigo, and P. Coppin, "An automated waveband selection technique for optimized hyperspectral mixture analysis," *Int. J. Remote Sens.*, vol. 31, pp. 5549–5568, 2010.

[17] B. Somers, S. Delalieux, J. Stuckens, W. W. Verstraeten, and P. Coppin, "A weighted linear spectral mixture analysis approach to address endmember variability in agricultural production systems," *Int. J. Remote Sens.*, vol. 30, pp. 139–147, 2009.

[18] G. P. Asner, D. E. Knapp, T. Kennedy-Bowdoin, M. O. Jones, R. E. Martin, J. Boardman, and R. F. Hughes, "Invasive species detection in Hawaiian rainforests using airborne imaging spectroscopy and LiDAR," *Remote Sens. Environ.*, vol. 112, pp. 1942–1955, 2008.

[19] G. P. Asner, R. F. Hughes, J. Mascaro, A. L. Uowolo, D. E. Knapp, J. Jacobson, T. Kennedy-Bowdoin, and J. K. Clark, "High-resolution carbon mapping on the million-hectare Island of Hawaii," *Frontiers in Ecology and Environment*, vol. 9, pp. 434–439, 2011.

[20] A. Plaza, P. Martinez, R. Perez, and J. Plaza, "A quantitative and comparative analysis of endmember extraction algorithms from hyperspectral data," *IEEE Trans. Geosci. Remote Sens.*, vol. 42, pp. 650–663, 2004.

[21] C. A. Bateson, G. P. Asner, and C. A. Wessman, "Endmember bundles: A new approach to incorporating endmember variability into spectral mixture analysis," *IEEE Trans. Geosci. Remote Sens.*, vol. 38, pp. 1083–1094, 2000.

[22] B. Somers, M. Zortea, A. Plaza, and G. P. Asner, "Automated extraction of image-based endmember bundles for improved spectral unmixing," *IEEE J. Sel. Topics Appl. Earth Observ. Remote Sens. (JSTARS)*, vol. 5, pp. 396–408.
[23] G. J. Fitzgerald, P. J. Pinter, D. J. Hunsaker, and T. R. Clarke, "Multiple shadow fractions in spectral mixture analysis of a cotton canopy," *Remote Sens. Environ.*, vol. 97, pp. 526–539, 2005.
[24] L. C. Plourde, S. V. Ollinger, M.-L. Smith, and M. E. Martin, "Estimating species abundance in a northern temperate forest using spectral mixture analysis," *Photogramm. Eng. Remote Sens.*, vol. 73, pp. 829–840, 2007.
[25] G. Bino, N. Levin, S. Darawshi, N. Van der Hal, A. Reich-Solomon, and S. Kark, "Accurate prediction of bird species richness patterns in an urban environment using Landsat-derived NDVI and spectral unmixing," *Int. J. Remote Sens.*, vol. 29, pp. 3675–3700, 2008.
[26] G. P. Guerschman, M. J. Hill, L. J. Renzullo, D. J. Barrett, A. S. Marks, and E. J. Botha, "Estimating fractional cover of photosynthetic vegetation, non-photosynthetic vegetation and bare soil in the Australian tropical savanna region upscaling the EO-1 Hyperion and MODIS sensors," *Remote Sens. Environ.*, vol. 113, pp. 928–945, 2009.
[27] F. Van der Meer and S. M. De Jong, "Improving the results of spectral unmixing of Landsat thematic mapper imagery by enhancing the orthogonality of endmembers," *Int. J. Remote Sens.*, vol. 21, pp. 2781–2797, 2000.
[28] C. H. Song, "Spectral mixture analysis for subpixel vegetation fractions in the urban environment: How to incorporate endmember variability?," *Remote Sens. Environ.*, vol. 95, pp. 248–263, 2005.
[29] G. P. Asner, D. E. Knapp, T. Kennedy-Bowdoin, M. O. Jones, R. E. Martin, J. Boardman, and C. B. Field, "Carnegie airborne observatory: In-flight fusion of hyperspectral imaging and waveform light detection and ranging (wLiDAR) for three-dimensional studies of ecosystems," *J. Appl. Remote Sens.*, vol. 1, no. 013536, 2007.
[30] R. Pouteau and B. Stoll, "SVM Selective Fusion (SELF) for multisource classification of structurally complex tropical rainfores," *IEEE J. Sel. Topics Appl. Earth Observ. Remote Sens. (JSTARS)*, doi 10.1109/JSTARS.2012.2183857.

Ben Somers received the M.Sc. and Ph.D. degree in bioscience engineering (land and forest management) from the Katholieke Universiteit Leuven (K. U. Leuven), Belgium, in 2005 and 2009, respectively.

In 2010 he was a research associate at the Geomatics Engineering group of the K. U. Leuven, Belgium. Since 2011 he has been a researcher at the Flemish Institute for Technological Research (VITO), Belgium. His research interests are the design of processing tools for hyperspectral remote sensing with a specific focus on spectral mixture analysis and its application in precision farming and forest ecology.

Gregory P. Asner is on the faculty of the Department of Global Ecology, Carnegie Institution for Science and the Environmental Earth System Science Department at Stanford University, Stanford, CA.

His research interests include ecosystem ecology, biogeochemistry and remote sensing. He develops new technologies for science-based conservation assessments of ecosystems including carbon emissions, hydrological function, and biological diversity.